Signal Processing 93 (2013) 3435–3448

Contents lists available at ScienceDirect

Signal Processing

journal homepage: www.elsevier.com/locate/sigpro

Direction of arrival estimation for more correlated sources than active sensors ☆

Dyonisius Dony Arianandа *, Geert Leus

Faculty of Electrical Engineering Mathematics and Computer Sciences, Delft University of Technology, Mekelweg 4, 2628 CD, Delft, Zuid Holland, The Netherlands

ARTICLE INFO

Article history:
Received 17 August 2012
Received in revised form
29 March 2013
Accepted 2 April 2013
Available online 19 April 2013

Keywords:
Dynamic array
Periodic scanning
More correlated sources than active sensors
Underlying array
Least squares
Sparsity-regularized least squares
Second-order statistics

ABSTRACT

In this paper, a new direction of arrival (DOA) estimation method for more correlated sources than active receiving antennas is proposed. The trick to solve this problem using only second-order statistics is to consider a periodic scanning of an underlying uniform array, where a single scanning period contains several time slots and in different time slots different sets of antennas are activated leading to a dynamic non-uniform array with possibly less active antennas than sources in each time slot. We collect the spatial correlation matrices of the active antenna arrays for all time slots and are able to present them as a linear function of the spatial correlation matrix of the underlying array. We provide a necessary and sufficient condition for this system of equations to be full column-rank, which allows for a least squares (LS) reconstruction of the spatial correlation matrix of the underlying array. Some practical greedy algorithms are presented to design dynamic arrays satisfying this condition. In a second step, we use the resulting spatial correlation matrix of the underlying array to estimate the DOAs of the possibly correlated sources by spatial smoothing and MUSIC. Alternatively, we can express this matrix as a linear function of the correlation matrix of the sources (incoming signals) at a grid of investigated angles, and solve this system of equations using either LS or sparsity-regularized LS (possibly assisted by additional constraints), depending on the grid resolution compared to the number of antennas of the underlying array.

1. Context

In this section, we present the underlying model that will be used in the next sections and discuss related work on direction of arrival (DOA) estimation. Here, we restrict our attention to deterministic methods as well as stochastic methods exploiting up to second-order statistics. The presented approaches are further classified into methods that can handle correlated sources as well as methods that can handle more sources than sensors.

To set the stage, let us consider a uniform array of N antennas receiving K narrowband signals produced by possibly correlated sources. For simplicity, we assume in this paper that this uniform array of N antennas is one-dimensional, i.e., we adopt a uniform linear array (ULA), but our exposition can be extended to higher dimensional arrays. The output of the ULA can be written as

$$\mathbf{x}(t) = \sum_{k=1}^{K} \mathbf{a}(\theta_k) s_k(t) + \mathbf{n}(t) = \mathbf{A}\mathbf{s}(t) + \mathbf{n}(t) \tag{1}$$

where t is the time index, $\mathbf{x}(t)$ is the $N \times 1$ output vector containing the received signals at the N antennas, $\mathbf{n}(t)$ is the $N \times 1$ noise vector containing the noises at the N

☆ This work is supported by NWO-STW under the VICI program (Project 10382). Part of this work appeared at the Asilomar Conference on Signals, Systems, and Computers, November 2012.

* Corresponding author. Tel.: +31 15 2781797; fax: +31 15 2786190.
E-mail addresses: d.a.dyonisius@tudelft.nl (D.D. Arianandа), g.j.t.leus@tudelft.nl (G. Leus).

0165-1684/$ - see front matter © 2013 Elsevier B.V. All rights reserved.
http://dx.doi.org/10.1016/j.sigpro.2013.04.011

antennas, $\mathbf{s}(t)=[s_1(t),s_2(t),\ldots,s_K(t)]^T$ is the $K\times 1$ source vector with $s_k(t)$ the incoming signal from the k-th source with angle θ_k, and $\mathbf{A}=[\mathbf{a}(\theta_1),\mathbf{a}(\theta_2),\ldots,\mathbf{a}(\theta_K)]$ is the $N\times K$ array response matrix with $\mathbf{a}(\theta_k)$ the array response vector for the k-th source. If we consider the first element of the ULA as a reference point, we can express the array response vector as $\mathbf{a}(\theta_k)=[1,\phi(\theta_k)^d,\phi(\theta_k)^{2d},\ldots,\phi(\theta_k)^{(N-1)d}]^T$, where d is the distance in wavelengths between two antennas and $\phi(\theta_k)=\exp(j2\pi\sin\theta_k)$. We always consider that $-\pi/2\le\theta_k<\pi/2$ and that $\{\theta_k\}_{k=1}^K$ contains different values. We generally assume that the impact of the wireless channel has been taken into account in $\mathbf{s}(t)$, that $\mathbf{n}(t)$ and $\mathbf{s}(t)$ are uncorrelated, and that the noises at the different antennas are mutually uncorrelated with variance σ_n^2, i.e., $E[\mathbf{n}(t)\mathbf{n}^H(t)]=\sigma_n^2\mathbf{I}_N$, with $\mathbf{I}_N$ the $N\times N$ identity matrix. However, the incoming signals can possibly be correlated with correlation matrix $E[\mathbf{s}(t)\mathbf{s}^H(t)]=\mathbf{R}_s$. As a result, the spatial correlation matrix $E[\mathbf{x}(t)\mathbf{x}^H(t)]=\mathbf{R}_x$ can be written as

$$\mathbf{R}_x=\mathbf{A}\mathbf{R}_s\mathbf{A}^H+\sigma_n^2\mathbf{I}_N. \tag{2}$$

To model the more general case of a non-uniform linear array (NULA), we can select M ($\le N$) antennas from the above ULA of N antennas, which is referred to as the *underlying array* in the following. Defining $\mathbf{y}(t)$ as the $M\times 1$ output vector representing the received signals at the M selected active antennas, we obtain

$$\mathbf{y}(t)=\mathbf{C}\mathbf{x}(t)=\sum_{k=1}^{K}\mathbf{b}(\theta_k)s_k(t)+\mathbf{m}(t)=\mathbf{B}\mathbf{s}(t)+\mathbf{m}(t), \tag{3}$$

where $\mathbf{C}$ is an $M\times N$ selection matrix containing M rows from $\mathbf{I}_N$, and where we further introduced $\mathbf{b}(\theta_k)=\mathbf{C}\mathbf{a}(\theta_k)$ and $\mathbf{B}=\mathbf{C}\mathbf{A}$ as the downsampled array response vector and matrix, respectively, which are both related to the set of M active antennas. Note that $\mathbf{m}(t)$ is the $M\times 1$ noise vector obtained as $\mathbf{m}(t)=\mathbf{C}\mathbf{n}(t)$, which has correlation matrix $E[\mathbf{m}(t)\mathbf{m}^H(t)]=\sigma_n^2\mathbf{I}_M$. The spatial correlation matrix of the active antennas can then be written as

$$\mathbf{R}_y=E[\mathbf{y}(t)\mathbf{y}^H(t)]=\mathbf{C}\mathbf{R}_x\mathbf{C}^H=\mathbf{B}\mathbf{R}_s\mathbf{B}^H+\sigma_n^2\mathbf{I}_M. \tag{4}$$

To retain the same aperture as the underlying ULA, we assume that $\mathbf{C}$ always selects the first and last antennas of the underlying ULA. We also assume that both the NULA and the underlying ULA introduce no spatial aliasing, which can be guaranteed by taking $d\le 1/2$ and by designing $\mathbf{C}$ such that the indices of the selected antennas are coprime [1], which is true for most existing NULA designs.

Based on the above model for a NULA, we will now discuss a number of state-of-the-art DOA estimation methods that can either handle correlated sources or more sources than sensors. Note that modeling a NULA by selecting a subset of antennas from a ULA turns out to be useful to explain some of the following DOA estimation methods. Moreover, the dynamic array concept we will propose in this paper will also build upon such a model, as will be explained in Section 2.

1.1. Handling correlated sources

Depending on the characteristics of the sources $\mathbf{s}(t)$ and the number of sources, K, relative to the total number of active antennas in the array, M, it is possible to perform DOA estimation based on $\mathbf{R}_y$ in (4) using existing approaches. It is clear that the signal correlation matrix $\mathbf{R}_s$ in (4) is diagonal when the incoming signals are uncorrelated, is nondiagonal and full rank when the signals are partially correlated, and is nondiagonal and rank deficient when the signals are fully correlated (coherent) [2]. When $\mathbf{R}_s$ has full rank and $M>K$, MUSIC in [3] (or root-MUSIC in [4]) can be applied. For uncorrelated or mildly correlated incoming signals, MUSIC performs very well but for highly or fully correlated signals, $\mathbf{R}_s$ in (4) is close to or exactly singular and the MUSIC performance deteriorates. As discussed in [5], for an array that contains a sufficient number of translational equivalent subarrays (this is for instance the case for a ULA, i.e., when we do not perform antenna selection and $\mathbf{C}=\mathbf{I}_N$), the highly or fully correlated sources in $\mathbf{s}(t)$ can be handled by applying the spatial smoothing preprocessing scheme in [2,6] to $\mathbf{R}_y$ in (4). This scheme leads to a spatially smoothed correlation matrix $\overline{\mathbf{R}}_y$ that can be expressed in terms of a full rank matrix $\overline{\mathbf{R}}_s$, which is a modified version of $\mathbf{R}_s$ in (4). Hence, MUSIC (or root-MUSIC) can now be applied to $\overline{\mathbf{R}}_y$. Interestingly, instead of using spatial smoothing and MUSIC to estimate the DOA of coherent incoming signals, [5] introduces a new method that relies on the evaluation of the distance between the investigated steering vectors and the subspace spanned by the columns of the product of the noise correlation matrix and the signal eigenvectors. This distance evaluation is based on the predefined distance metric called normalized distance functional. For another class of approaches, a fine grid of investigated angles is defined in the angular domain and then the output of the array is expressed in terms of a linear combination of the steering vectors of these investigated angles. For the model in (3), this is equivalent to writing $\mathbf{y}(t)$ as

$$\mathbf{y}(t)=\sum_{q=1}^{Q}\mathbf{b}(\tilde{\theta}_q)s_{\tilde{\theta}_q}(t)+\mathbf{m}(t)=\tilde{\mathbf{B}}\tilde{\mathbf{s}}(t)+\mathbf{m}(t), \tag{5}$$

where $\tilde{\mathbf{s}}(t)=[s_{\tilde{\theta}_1}(t),s_{\tilde{\theta}_2}(t),\ldots,s_{\tilde{\theta}_Q}(t)]^T$ is the $Q\times 1$ extended source vector with $s_{\tilde{\theta}_q}(t)$ the incoming signal from the q-th investigated angle $\tilde{\theta}_q$, and $\tilde{\mathbf{B}}=[\mathbf{b}(\tilde{\theta}_1),\mathbf{b}(\tilde{\theta}_2),\ldots,\mathbf{b}(\tilde{\theta}_Q)]$ is the $M\times Q$ extended subsampled array response matrix with $\mathbf{b}(\tilde{\theta}_q)$ the subsampled array response vector for the q-th investigated angle $\tilde{\theta}_q$. As before, we always consider that $-\pi/2\le\tilde{\theta}_q<\pi/2$ and that $\{\tilde{\theta}_q\}_{q=1}^Q$ contains different values. It is important to note that $\{\tilde{\theta}_q\}_{q=1}^Q$ is known and might approximately contain the set of actual angles of arrival $\{\theta_k\}_{k=1}^K$ contained in $\mathbf{B}$ in (3), which is not known by the receiver. Based on (5) and defining the extended source correlation matrix as $E[\tilde{\mathbf{s}}(t)\tilde{\mathbf{s}}(t)^H]=\mathbf{R}_{\tilde{s}}$, we can also express $\mathbf{R}_y$ in (4) as

$$\mathbf{R}_y=\tilde{\mathbf{B}}\mathbf{R}_{\tilde{s}}\tilde{\mathbf{B}}^H+\sigma_n^2\mathbf{I}_M. \tag{6}$$

The DOA estimation approach proposed in [7] exploits the model described by (5) with $Q\gg M$. In this case, $\tilde{\mathbf{B}}$ has more columns than rows and as a result, the columns of $\tilde{\mathbf{B}}$ play the role of an overcomplete basis for $\mathbf{y}(t)$. To overcome this problem, [7] assumes that the coefficient vector with respect to this overcomplete basis is generally sparse. Further, [7] exploits multiple measurement vectors (MMV)

by collecting data from multiple time indices, based on the assumption that the DOAs do not change within the duration of the sample acquisition. Hence, their data model is given by $\mathbf{Y}=\tilde{\mathbf{B}}\tilde{\mathbf{S}}+\mathbf{M}$, where $\mathbf{Y}$, $\mathbf{M}$, and $\tilde{\mathbf{S}}$ respectively stack $\mathbf{y}(t)$, $\mathbf{m}(t)$ and $\tilde{\mathbf{s}}(t)$ over different time indices in a row-wise fashion. Next, the so-called ℓ_1 singular value decomposition (ℓ_1−SVD) algorithm consisting of a dimensionality reduction of the MMV model as well as a mixed $\ell_{2,1}$−norm minimization is used to exploit the group sparsity of the columns of $\tilde{\mathbf{S}}$ in the MMV model. A closely related method can be found in [8], with the difference that a mixed $\ell_{2,0}$−norm approximation is used instead of a mixed $\ell_{2,1}$−norm to exploit the group sparsity of the columns of $\tilde{\mathbf{S}}$, leading to the so-called joint ℓ_0 approximation (JLZA) algorithm.

Other grid-based methods directly exploit (6) again with $Q \gg M$, such as the work of [9]. There, the columns of $\tilde{\mathbf{B}}$ play the role of overcomplete basis for each column of $\mathbf{R}_y$ and as before sparsity is assumed in the coefficient vector corresponding to this basis. Since all columns of $\mathbf{R}_y$ have the same sparse structure with respect to this overcomplete basis, group sparsity is again exploited to estimate the DOA of the incoming signals leading to the so-called ℓ_1 sparse representation of array covariance vectors (ℓ_1−SRACV) algorithm. As the ℓ_1−SVD and JLZA algorithms, the ℓ_1−SRACV algorithm is robust to the correlation of the incoming signals. The model in (6) is also exploited in [10,11], where a spatial correlation matching approach is considered. The resulting so-called sparse iterative covariance-based estimation (SPICE) method is derived assuming uncorrelated sources and sparsity of the sources in the angular domain, i.e., the extended source correlation matrix $\mathbf{R}_{\tilde{s}}$ in (6) is diagonal with only a few non-zero diagonal elements. Although SPICE has been derived based on uncorrelated sources, it has been shown to be robust against correlation.

1.2. Handling more sources than sensors

Most of the aforementioned methods can handle correlated sources, but they generally require more active antennas than sources ($M \geq K$). This is understandable for those methods involving the use of MUSIC, and it has also been shown to hold for the grid-based methods exploiting sparsity, which actually require $M \geq 2K$. For uncorrelated sources, on the other hand, some approaches have been proposed for DOA estimation when there are more sources than physical receiving antennas. One example in [12,13] exploits the Caratheodory theorem and constructs the so-called augmented correlation matrix from the spatial correlation matrix. However, they rely on the exact knowledge of the spatial correlation matrix, which is unavailable in practice and has to be estimated from sample averaging. When this is the case, the augmented correlation matrix might not be positive semi-definite, i.e., it might not be a valid correlation matrix, thereby leading to a performance degradation. In [14], a complex algorithm has been introduced to convert the augmented correlation matrix into a valid positive semi-definite correlation matrix.

More popular techniques for uncorrelated sources exploit the fact that the source correlation matrix $\mathbf{R}_s$ is diagonal and rewrite (4) as

$$\mathrm{vec}(\mathbf{R}_y)=(\mathbf{B}^*\odot\mathbf{B})\mathrm{diag}(\mathbf{R}_s)+\sigma_n^2\mathrm{vec}(\mathbf{I}_M) \tag{7}$$

where $\odot$ denotes the Khatri-Rao product operation and $\mathrm{vec}(\cdot)$ is the operator that cascades all columns of a matrix in a large column vector. Observe that the N_v distinct rows of $\mathbf{B}^*\odot\mathbf{B}$ provide the array response matrix of a virtual array (also known as co-array) of N_v virtual antennas receiving K virtual sources at the angles $\{\theta_k\}_{k=1}^{K}$ (note that generally $N_v > M$ and the upper bound is given by $N_v \leq M(M-1)+1$). The problem now is that only a single measurement vector is available and thus the behavior of the model (7) is similar to an array receiving constant and hence fully coherent source signals, which is problematic for DOA estimation. A first method to solve this issue relies on the assumption that $\mathrm{diag}(\mathbf{R}_s)$, and thus $\mathrm{vec}(\mathbf{R}_y)$, is time-varying, which basically means that quasi-stationary sources are assumed and thus enough linearly independent measurement vectors can be obtained [15]. But it is clear that this method will fail in case of stationary sources, which was the starting point of this paper. A second technique again relies on gridding and exploits the model (6), which for uncorrelated sources can be written as

$$\mathrm{vec}(\mathbf{R}_y)=(\tilde{\mathbf{B}}^*\odot\tilde{\mathbf{B}})\mathrm{diag}(\mathbf{R}_{\tilde{s}})+\sigma_n^2\mathrm{vec}(\mathbf{I}_M). \tag{8}$$

If we select the angular resolution such that $Q=N_v$, we can solve (8) using ordinary least squares (LS) [16]. This is particularly interesting if we want to obtain an analytical performance analysis of the solution. However, when N_v is too small, this leads to a bad angular resolution and it will be difficult to estimate the DOA of off-grid sources. The other option is to take a fine grid of investigated angles, for which $Q > N_v$. In that case, we have to rely on the sparsity (possibly assisted by the positivity) of $\mathrm{diag}(\mathbf{R}_{\tilde{s}})$ to solve the underdetermined problem (8), as was recently advocated in [17]. A final technique is based on constructing special array geometries of M antennas, through the design of the selection matrix $\mathbf{C}$ in (3), such that the overall virtual array of N_v antennas subsumes a ULA of N_u antennas, referred to as the virtual ULA, where generally $M < N_u \leq N_v$. Examples of such array designs are the two-level nested array [18], the coprime array [19], and the minimal sparse ruler array [16]. Under this virtual ULA, the DOAs can again be estimated using gridding and adopting the earlier mentioned LS [16] or sparsity-constrained LS (possibly assisted by a positivity constraint) [17]. Different from a general virtual array, $\tilde{\mathbf{B}}^*\odot\tilde{\mathbf{B}}$ now has a Vandermonde structure, which simplifies the implementation and analysis of these methods. Alternatively, it is now also possible to apply spatial smoothing and MUSIC based on the single available measurement vector from the virtual ULA.

1.3. Handling more correlated sources than sensors

All the above methods either focus on correlated sources, but then the upper bound of the number of sources is lower than the number of antennas, or they focus on detecting more uncorrelated sources than sensors. To the best of our knowledge, there are no deterministic or stochastic methods using up to second-order

statistics that can handle more correlated sources than sensors. Only higher-order statistics have been exploited up to now to solve this problem (see e.g. [20]). In this paper, we will fill this gap, and introduce a new approach to tackle more correlated sources than *active* sensors. The paradigm shift introduced to reach this goal is to periodically change the selection of the M active antennas from the underlying ULA of N antennas. This will be explained in detail in the following sections.

2. Dynamic array through periodic scanning

In this section, we introduce a novel dynamic array for DOA estimation of possibly correlated or even fully coherent signals when the number of sources is more than the number of active antennas at any given time. The underlying ULA consisting of N antennas discussed in Section 1 is used as an array of available antennas from which we activate only M antennas within a specific time slot, where the set of M activated antennas can differ from time slot to time slot. In this way, even though the number of required physical antennas is equal to N, the number of active antennas per time slot, and thus the number of hardware receiver branches, is reduced from N to M. This scheme reduces the power consumption without compromising the ability to locate the DOAs of the sources. In other words, the number of sources we will be able to detect is the same as if we had all N antennas from the underlying ULA available all the time. Note that instead of antenna switching, we can equivalently employ $M<N$ adjustable antennas to construct a dynamic array allowing us to alter the position of each antenna in every time slot.

Let us now discuss the conceived dynamic array in some more detail. We basically focus on some kind of periodic scanning with P scanning periods, where a single scanning period consists of L time slots, and where a single time slot consists of S samples (see Fig. 1). The set of M activated antennas within a single scanning period is different from time slot to time slot whereas the set of active antennas in the l-th time slot of different scanning periods is the same. Defining $\mathbf{x}(t)$ as the output vector of the underlying ULA of N antennas, as in Section 1, and assuming for simplicity that the sample period is 1, we introduce $\mathbf{y}_l(\tau)$ as the $M\times 1$ vector representing the output of the M active antennas of the linear array in the l-th time slot ($l=0,1,\ldots,L-1$), which is given by

$$\mathbf{y}_l(\tau)=\mathbf{C}_l\mathbf{x}(pLS+lS+s)$$

where $\lfloor \tau/S \rfloor = p$ ($p=0,1,\ldots,P-1$) indicates the scanning period index, $s=\tau-pS$ ($s=0,1,\ldots,S-1$) indicates the sample index within the l-th time slot of the $p-$th scanning period, and where the $M\times N$ matrix $\mathbf{C}_l$ is constructed by selecting M out of N rows from the identity matrix $\mathbf{I}_N$. Note that the indices of the M selected rows represent the indices of the M active antennas in the l-th time slot selected from the N available antennas in the underlying ULA. We are then able to compute the $M\times M$ spatial correlation matrix of $\mathbf{y}_l(\tau)$ as

$$\mathbf{R}_{y_l}=E[\mathbf{y}_l(\tau)\mathbf{y}_l(\tau)^H]=\mathbf{C}_l\mathbf{R}_x\mathbf{C}_l^T \tag{9}$$

where the second equality is due to the fact that $\mathbf{C}_l$ is a real matrix. Note that the expectation operation in (9) can be estimated by taking an average over PS time samples. Next, let us stack all columns of $\mathbf{R}_{y_l}$ into the $M^2\times 1$ vector vec ($\mathbf{R}_{y_l}$). Based on (9), we can then express vec ($\mathbf{R}_{y_l}$) as

$$\mathbf{r}_{y_l}=\mathrm{vec}(\mathbf{R}_{y_l})=(\mathbf{C}_l\otimes\mathbf{C}_l)\mathrm{vec}(\mathbf{R}_x) \tag{10}$$

where $\otimes$ denotes the Kronecker product operation. Finally, we can combine $\mathbf{r}_{y_l}$ in (10) for all time slots $l=0,1,\ldots,L-1$ into a single vector $\mathbf{r}_y$, which is given by $\mathbf{r}_y=[\mathbf{r}_{y_0}^T,\mathbf{r}_{y_1}^T,\ldots,\mathbf{r}_{y_{L-1}}^T]^T$. The relationship between $\mathbf{r}_y$ and $\mathbf{R}_x$ is then provided by

$$\mathbf{r}_y=\boldsymbol{\Psi}\,\mathrm{vec}(\mathbf{R}_x) \tag{11}$$

where the $M^2L\times N^2$ matrix $\boldsymbol{\Psi}$ is given by

$$\boldsymbol{\Psi}=[(\mathbf{C}_0\otimes\mathbf{C}_0)^T,(\mathbf{C}_1\otimes\mathbf{C}_1)^T,\ldots,(\mathbf{C}_{L-1}\otimes\mathbf{C}_{L-1})^T]^T. \tag{12}$$

This equation forms the basis of this paper and it allows for the reconstruction of vec($\mathbf{R}_x$) from $\mathbf{r}_y$, which will be discussed in the next section.

3. Reconstruction of spatial correlation matrix $\mathbf{R}_x$

One option to solve (11) is using ordinary LS. If $\boldsymbol{\Psi}$ has full column rank, we then obtain

$$\mathrm{vec}(\hat{\mathbf{R}}_x)=(\boldsymbol{\Psi}^T\boldsymbol{\Psi})^{-1}\boldsymbol{\Psi}^T\mathbf{r}_y. \tag{13}$$

Alternatively, we could add a positive semi-definite (p.s.d.) constraint on $\mathbf{R}_x$ in the aforementioned ordinary LS problem, leading to the following constrained LS reconstruction

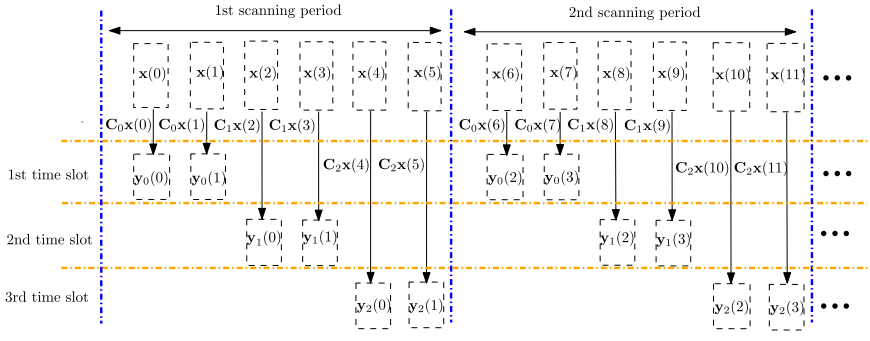

Fig. 1. Description of the periodic scanning process where a single scanning period consists of L time slots. Here the number of time slots per scanning period is $L=3$ and the number of samples per slot per antenna is given by $S=2$.

problem:

$$\hat{\mathbf{R}}_x = \arg\min_{\mathbf{R}_x} \|\mathbf{r}_y - \boldsymbol{\Psi}\,\mathrm{vec}(\mathbf{R}_x)\|_2^2 \quad \text{s.t. } \mathbf{R}_x \succcurlyeq \mathbf{0}_{N\times N}, \tag{14}$$

where $\mathbf{0}_{m\times n}$ denotes an $m \times n$ matrix containing only zeros. This could possibly alleviate the requirement of a full column rank $\boldsymbol{\Psi}$, but comes at the expense of a large computational complexity. Either way, it is still of great interest to design $\{\mathbf{C}_l\}_{l=0}^{L-1}$ such that $\boldsymbol{\Psi}$ has full column rank, which clearly requires $M^2L \geq N^2$. Observe that, since $M < N$, we can only have $M^2L \geq N^2$ if at least two time slots per scanning period are adopted, i.e., $L \geq 2$. In other words, a dynamic array through periodic scanning is indispensable for generating a full column rank $\boldsymbol{\Psi}$.

In the remainder of this section, we will first propose a necessary and sufficient condition for the periodic subsampling procedure to have a full column rank $\boldsymbol{\Psi}$ in (12). Next, we will develop some practical greedy approaches to design a periodic scanning scheme that satisfies this condition. Finally, we will discuss some trade-offs related to the design of the dynamic array.

3.1. Establishing perfect reconstruction

In order to simplify our analysis, let us start by introducing the following lemma.

Lemma 1. *$\mathbf{C}_l \otimes \mathbf{C}_l$ will have a one in the $[(i-1)N+j]$−th and $[(j-1)N+i]$−th columns if and only if $\mathbf{C}_l$ contains the i-th and j-th rows of the identity matrix $\mathbf{I}_N$.*

The proof of this lemma can be found in Appendix A. This lemma directly implies the following corollary.

Corollary 1. *If $\mathbf{C}_l$ is constructed by selecting M different rows of $\mathbf{I}_N$, the rows of $\mathbf{C}_l \otimes \mathbf{C}_l$ have a single one at exactly M^2 different positions. Out of the M^2 rows of $\mathbf{C}_l \otimes \mathbf{C}_l$, M rows are produced by the self-Kronecker product of every row of $\mathbf{C}_l$. On the other hand, every pair of two different rows of $\mathbf{C}_l$ contributes to two different rows of $\mathbf{C}_l \otimes \mathbf{C}_l$, each of which has a single one at a different position. Since we have $\binom{M}{2}$ possible combinations of two different rows, all Kronecker products between any two different rows of $\mathbf{C}_l$ lead to $M(M-1)$ rows of $\mathbf{C}_l \otimes \mathbf{C}_l$, all of which have a single one at a different position.*

Let us now define Γ_l as the set of M indices selected from $\{1, 2, \ldots, N\}$ representing the rows of $\mathbf{I}_N$ that we use to construct $\mathbf{C}_l$. Then, the set of the M^2 indices of the columns of $\mathbf{C}_l \otimes \mathbf{C}_l$ that contain a one is provided by

$$\Omega_l = \{(i-1)N + j \,|\, i, j \in \Gamma_l\}. \tag{15}$$

Since every row of $\mathbf{C}_l \otimes \mathbf{C}_l$ has only a single one, it is clear from (12) that every row of $\boldsymbol{\Psi}$ also has only a single one. As a result, $\boldsymbol{\Psi}$ will have full column rank if and only if each of its columns has at least a single one, which from (12) and (15) is equivalent to

$$\bigcup_{l=0}^{L-1} \Omega_l = \{1, 2, \ldots, N^2\}. \tag{16}$$

This result leads to the following theorem.

Theorem 1. *$\boldsymbol{\Psi}$ in (12) has full column rank if and only if every possible combination of two antennas in the underlying ULA is active in at least one of the L possible time slots within a single scanning period.*

Proof. Note that the condition in Theorem 1 is equivalent to using every possible pair of two different rows of $\mathbf{I}_N$ in at least one of the L possible matrices $\{\mathbf{C}_l\}_{l=0}^{L-1}$. Based on Lemma 1 and Corollary 1, this will guarantee that the $[(i-1)N+j]$−th and the $[(j-1)N+i]$−th columns of $\boldsymbol{\Psi}$ have at least a single one for all $i, j \in \{1, \ldots, N\}$. This proves the sufficiency part of the theorem. In order to prove the necessity part, let us assume that $\boldsymbol{\Psi}$ in (12) has full column rank and that the a-th and b-th antennas in the underlying ULA are never simultaneously active in the same time slot. This equivalently means that none of the matrices $\{\mathbf{C}_l\}_{l=0}^{L-1}$ contains both the a-th and b-th rows of the identity matrix $\mathbf{I}_N$. According to Lemma 1 and using (12), it is then obvious that the $[(a-1)N+b]$−th and the $[(b-1)N+a]$−th columns of $\boldsymbol{\Psi}$ only contain zeros and thus $\boldsymbol{\Psi}$ does not have full column rank, which contradicts the initial assumption. This concludes the proof. □

Note that Theorem 1 automatically requires $M \geq 2$. Further note that since each row of $\boldsymbol{\Psi}$ only contains a single one and zeros elsewhere, the reconstruction of $\mathrm{vec}(\mathbf{R}_x)$ using ordinary LS as in (13) is computationally easy to perform.

3.2. Greedy dynamic array design

As we will discuss in Section 3.3, subject to the full column rank condition of $\boldsymbol{\Psi}$, it is generally not possible to minimize both the number of active antennas per time slot M and the number of time slots per scanning period L simultaneously. In this section, we discuss a greedy dynamic array design that aims to either minimize M given L or minimize L given M subject to (16).

Based on Theorem 1, we first try to minimize L given M subject to (16) by defining Λ as $\Lambda = \{(i,j) | i, j \in \{1, 2, \ldots, N\}, i < j\}$ and Λ_l as the set of all possible combinations of two row indices of $\mathbf{I}_N$ that are used to construct $\mathbf{C}_l$, that is

$$\Lambda_l = \{(i,j) | i, j \in \Gamma_l, i < j\}.$$

Our task to minimize L given M subject to (16) can now be expressed as

$$\min_{L, \{\Gamma_l\}_{l=0}^{L-1}} L \quad \text{subject to} \quad \bigcup_{l=0}^{L-1} \Lambda_l = \Lambda \ \text{ and } \ |\Gamma_l| = M, \ \forall l \tag{17}$$

where $|\Gamma_l|$ denotes the cardinality of the set Γ_l. The minimization problem in (17) is generally a non-trivial combinatorial problem. However, it is possible to find a lower bound for L. Note that $|\Lambda| = N(N-1)/2$ and $|\Lambda_l| = M(M-1)/2$. It is then clear that L is lower bounded by

$$L \geq \left\lceil \frac{|\Lambda|}{|\Lambda_l|} \right\rceil = \left\lceil \frac{N(N-1)}{M(M-1)} \right\rceil \tag{18}$$

where $\lceil x \rceil$ denotes the smallest integer not smaller than x. While the minimization problem in (17) is generally hard to solve, we propose a greedy algorithm to find a suboptimal solution for L and $\{\Gamma_l\}_{l=0}^{L-1}$ given M subject to (16).

This algorithm, called Algorithm 1, is described in Table 1 and its explanation is provided in Appendix B.

Similarly, given a certain value of L, the minimization of M subject to (16) can be stated as

$$\min_{M,\{\Gamma_l\}_{l=0}^{L-1}} M \quad \text{subject to} \quad \bigcup_{l=0}^{L-1} \Lambda_l = \Lambda \quad \text{and} \quad |\Gamma_l| = M, \ \forall l.$$

In this case, the lower bound for M is given by

$$\frac{M^2-M}{2} \geq \left\lceil \frac{|\Lambda|}{L} \right\rceil = \left\lceil \frac{N(N-1)}{2L} \right\rceil. \tag{19}$$

We also propose a greedy algorithm to find a sub-optimal solution for M and $\{\Gamma_l\}_{l=0}^{L-1}$ given L subject to (16). This algorithm, called Algorithm 2, is described in Table 2 and its explanation is provided in Appendix C.

3.3. Trade-offs for dynamic array design

While we want to achieve (16) to ensure the full column rank condition of Ψ, we also want to keep the computational complexity low, the number of active antennas and hardware receiver branches M small, and the number of antenna reconfigurations L within a scanning

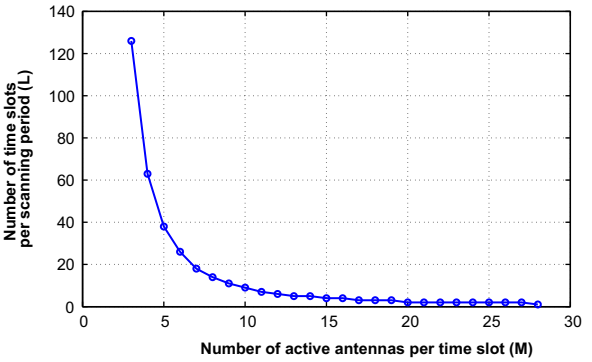

Fig. 2. Illustration of the trade-off between the number of active antennas M and a lower bound on the number of time slots per scanning period L. Here, we have $N=28$.

Table 1
Algorithm 1: A greedy algorithm to find a sub-optimal solution for L and $\{\Gamma_l\}_{l=0}^{L-1}$ given M subject to (16).

Algorithm 1

Introduce $\mathbf{Z}^{(f)}$ as an $N \times N$ indicator matrix at the f-th iteration and denote its element at the i-th row and the j-th column by $[\mathbf{Z}^{(f)}]_{i,j}$.
Initialize $f=0$ and $\mathbf{Z}^{(0)} = \mathbf{I}_N$.
While $\mathbf{Z}^{(f)}$ has at least one zero entry do
    Set $f = f+1$ and $\mathbf{Z}^{(f)} = \mathbf{Z}^{(f-1)}$.
    Randomly select $i,j \in \{1,2,\ldots,N\}$ for which $[\mathbf{Z}^{(f)}]_{i,j} = 0$ and set $\Gamma_{f-1} = \{i,j\}$. Then also set both $[\mathbf{Z}^{(f)}]_{i,j}$ and $[\mathbf{Z}^{(f)}]_{j,i}$ to 1.
    for $\kappa = 1$ to $M-2$ do
        Define a set $\Xi = \{1,2,\ldots,N\} \backslash \Gamma_{f-1}$.
        Search in Ξ for the element g that satisfies: $g = \arg\min_{g' \in \Xi} \sum_{i' \in \Gamma_{f-1}} [\mathbf{Z}^{(f)}]_{i',g'}$.
        For all $i' \in \Gamma_{f-1}$ set $[\mathbf{Z}^{(f)}]_{i',g}$ and $[\mathbf{Z}^{(f)}]_{g,i'}$ to 1.
        Update Γ_{f-1} to $\Gamma_{f-1} = \Gamma_{f-1} \bigcup \{g\}$.
    end for
end while
The value of L is given by $L=f$ and the output of this algorithm is $\{\Gamma_l\}_{l=0}^{L-1}$.

Table 2
Algorithm 2: A greedy algorithm to find a sub-optimal solution for M and $\{\Gamma_l\}_{l=0}^{L-1}$ given L subject to (16).

Algorithm 2

Introduce $\mathbf{Z}^{(f)}$ as an $N \times N$ indicator matrix at the f-th iteration and denote its element at the i-th row and the j-th column by $[\mathbf{Z}^{(f)}]_{i,j}$.
Initialize $f=0$ and $\mathbf{Z}^{(0)} = \mathbf{I}_N$.
Set $f = f+1$ and $\mathbf{Z}^{(f)} = \mathbf{Z}^{(f-1)}$.
for $l=0$ to $L-1$ do
    Randomly select $i,j \in \{1,2,\ldots,N\}$ for which $[\mathbf{Z}^{(f)}]_{i,j} = 0$ and set $\Gamma_l = \{i,j\}$.
    Set both $[\mathbf{Z}^{(f)}]_{i,j}$ and $[\mathbf{Z}^{(f)}]_{j,i}$ to 1.
end for
While $\mathbf{Z}^{(f)}$ has at least one zero entry do
    Set $f = f+1$ and then set $\mathbf{Z}^{(f)} = \mathbf{Z}^{(f-1)}$.
    for $\kappa = 0$ to $L-1$ do
        Define a set $\Xi = \{1,2,\ldots,N\} \backslash \Gamma_\kappa$.
        Search in Ξ for the element g that satisfies: $g = \arg\min_{g' \in \Xi} \sum_{i' \in \Gamma_\kappa} [\mathbf{Z}^{(f)}]_{i',g'}$.
        For all $i' \in \Gamma_\kappa$ set $[\mathbf{Z}^{(f)}]_{i',g}$ and $[\mathbf{Z}^{(f)}]_{g,i'}$ to 1.
        Update Γ_κ to $\Gamma_\kappa = \Gamma_\kappa \bigcup \{g\}$.
    end for
end while
The value of M is given by $M = f+1$ and the output of this algorithm is $\{\Gamma_l\}_{l=0}^{L-1}$.

period minimal. However, it turns out that simultaneously minimizing everything is not possible. Let us consider the following trade-offs.

Corollary 1 implies that, for each value of $l\in\{0,1,\ldots,L-1\}$, only M^2 out of N^2 columns of $\mathbf{C}_l\otimes\mathbf{C}_l$ have at least a single non-zero element. Minimizing M will decrease the number of non-zero columns of $\mathbf{C}_l\otimes\mathbf{C}_l$. As a result, in order to ensure that all columns of $\boldsymbol{\Psi}$ in (12) have at least a single non-zero element, we need a larger L. This means that there is a trade-off between M and L for a given amount of time within a scanning period. Fig. 2 illustrates the trade-off between M and L for $N=28$ where we vary M from 3 to 28. The value of L is computed by using the lower bound formula given by (18) to simplify the illustration. As a final remark on the trade-off between M and L, it is also important to observe from (11) that the size of $\boldsymbol{\Psi}$ to be inverted depends quadratically on M and only linearly on L.

Secondly, consider the relation between L, M, the number of scanning periods P, and the total number of received samples per time slot per antenna S. Recall that the larger PS the better the quality of the estimate of $\mathbf{R}_{y_l}$ in (9). If we have a fixed total sensing time (which implies a given PSL), a larger PS implies a smaller L, which in turn, also implies a larger number of antennas M that need to be activated in each time slot. Hence, for a given total sensing time PSL, we have a trade-off between M and the quality of the estimate of $\mathbf{R}_{y_l}$ in (9). This trade-off can also be illustrated in Fig. 2. For example, by fixing PSL to $PSL\approx\alpha$, we can compute for every value of PS the corresponding value of L as $L=\text{round}(\alpha/(PS))$ and relate this to a value of M from Fig. 2.

Alternatively, we might also require a certain quality for the estimate of $\mathbf{R}_{y_l}$ in (9) and fix PS. In this case, the trade-off now is between M and the total sensing time PSL. Again, we can use Fig. 2 to illustrate this trade-off. For example, by fixing PS to $PS\approx\beta$, we can compute for every value of PSL the corresponding value of L as $L=\text{round}(PSL/\beta)$ and relate this to a value of M from Fig. 2.

4. Source correlation reconstruction and direction of arrival estimation

After the reconstruction of $\mathbf{R}_x$, any covariance-based method capable of handling correlated sources from Section 1.1 assuming no subsampling, i.e., $\mathbf{C}=\mathbf{I}_N$, can basically be used for DOA estimation. Examples are the spatial smoothing and MUSIC (or root-MUSIC) approach of [2,6], the ℓ_1−SRACV method of [9], or possibly SPICE [10,11]. In addition, we here also introduce some new covariance-based approaches which again rely on gridding the angular domain.

4.1. Least squares approach

The first possible approach is based on defining a grid of investigated angles in the angular domain and using a model similar to (6) but now with no subsampling, i.e., $\mathbf{C}=\mathbf{I}_N$. Using this model and taking (2) into account, we can write

$$\text{vec}(\mathbf{R}_x)=(\tilde{\mathbf{A}}^*\otimes\tilde{\mathbf{A}})\text{vec}(\mathbf{R}_{\tilde{s}})+\sigma_n^2\text{vec}(\mathbf{I}_N) \tag{20}$$

where $\tilde{\mathbf{A}}=[\mathbf{a}(\tilde{\theta}_1),\mathbf{a}(\tilde{\theta}_2),\ldots,\mathbf{a}(\tilde{\theta}_Q)]$ is the $N\times Q$ extended array response matrix for the underlying ULA with $\mathbf{a}(\tilde{\theta}_q)$ the array response vector for the q-th investigated angle $\tilde{\theta}_q$. From (20), we can reconstruct $\text{vec}(\mathbf{R}_{\tilde{s}})$ from $\text{vec}(\mathbf{R}_x)$ using LS, under the assumption that $\tilde{\mathbf{A}}$ in (20) has full column rank, which is only possible if $N\geq Q$. Assuming that $\tilde{\mathbf{A}}$ has full column rank, solving (20) using LS leads to

$$\text{vec}(\hat{\mathbf{R}}_{\tilde{s}})=((\tilde{\mathbf{A}}^*\otimes\tilde{\mathbf{A}})^H(\tilde{\mathbf{A}}^*\otimes\tilde{\mathbf{A}}))^{-1}(\tilde{\mathbf{A}}^*\otimes\tilde{\mathbf{A}})^H\text{vec}(\mathbf{R}_x). \tag{21}$$

Because of the Vandermonde structure of $\tilde{\mathbf{A}}$, it will always have full column rank if we take $N\geq Q$. However, in order to obtain a well-conditioned $\tilde{\mathbf{A}}$, we can take $N=Q$, use a half wavelength spacing ($d=0.5$) for the underlying ULA in (1), and adopt an inverse sinusoidal angular grid where the investigated angles $\tilde{\theta}_q$ are defined as

$$\tilde{\theta}_q=\sin^{-1}\left(\frac{2}{Q}\left(q-1-\left\lceil\frac{Q-1}{2}\right\rceil\right)\right),\quad q=1,2,\ldots,Q. \tag{22}$$

We can then easily derive that $\tilde{\mathbf{A}}$ is a permuted version of the inverse discrete Fourier transform (IDFT) matrix, which is a unitary matrix that does not introduce any noise enhancement when inverting the matrix. Furthermore, this also means that applying the inverse of $\tilde{\mathbf{A}}^*\otimes\tilde{\mathbf{A}}$ to a vector can easily be computed using fast Fourier transform (FFT) operations, leading to a complexity of order $N^2\log N$. The diagonal of the computed estimate of the correlation matrix $\hat{\mathbf{R}}_{\tilde{s}}$ indicates the received power at the investigated angles $\{\tilde{\theta}_q\}_{q=1}^{Q}$. Therefore, $\text{diag}(\hat{\mathbf{R}}_{\tilde{s}})$ can be perceived as the angular power spectrum estimate. The estimates of the actual DOAs can be found by locating the peaks of this angular power spectrum estimate. The off-diagonal components of $\hat{\mathbf{R}}_{\tilde{s}}$, on the other hand, reveal the correlations between the signals at the different investigated angles.

4.2. Sparsity-regularized least squares approach

As the number of investigated angles Q reduces, the probability that the DOA of a particular point source k is not located on or nearby a grid point increases. Since the LS approach requires $N\geq Q$, when N is small, Q will be small and the angular resolution of the LS estimate is poor and it will be challenging to estimate the DOA of off-grid point sources. One way to mitigate this problem is to take a finer grid of investigated angles by allowing $Q>N$. When this is the case, the resulting $\tilde{\mathbf{A}}^*\otimes\tilde{\mathbf{A}}$ in (20) is a wide matrix and its columns play the role of an overcomplete basis for $\text{vec}(\mathbf{R}_x)$ in (20). In order to solve the resulting underdetermined problem, a popular idea is to assume that $\text{vec}(\mathbf{R}_{\tilde{s}})$ is generally sparse and formulate the estimate of $\mathbf{R}_{\tilde{s}}$ as a solution of the sparsity-regularized LS problem:

$$\hat{\mathbf{R}}_{\tilde{s}}=\arg\min_{\mathbf{R}_{\tilde{s}}}\|\text{vec}(\mathbf{R}_x)-(\tilde{\mathbf{A}}^*\otimes\tilde{\mathbf{A}})\text{vec}(\mathbf{R}_{\tilde{s}})\|_2^2+\lambda\|\text{vec}(\mathbf{R}_{\tilde{s}})\|_1 \tag{23}$$

where the weight $\lambda\geq 0$ balances the sparsity-bias tradeoff. This can be regarded as an extension of the method proposed in [17], which is designed to handle only uncorrelated sources.

In the noiseless case, it is interesting to discuss conditions on $\tilde{\mathbf{A}}^*\otimes\tilde{\mathbf{A}}$ that guarantee perfect reconstruction of $\text{vec}(\mathbf{R}_{\tilde{s}})$ in (23). If the number of pairs of correlated sources

is given by K', then it is clear that $\mathrm{vec}(\mathbf{R}_{\tilde{s}})$ is a $\tilde{K}$-sparse vector, i.e., it has at most $\tilde{K}$ non-zero elements where $\tilde{K}=K+2K'$. The worst case occurs when $\tilde{K}=K^2$, i.e., each source is highly correlated to the other $K-1$ sources. When we try to recover $\mathrm{vec}(\mathbf{R}_{\tilde{s}})$ from $\mathrm{vec}(\mathbf{R}_x)$ using ℓ_0-norm minimization, it is well known that the Kruskal rank of $\tilde{\mathbf{A}}^*\otimes\tilde{\mathbf{A}}$ should satisfy $\mathrm{krank}(\tilde{\mathbf{A}}^*\otimes\tilde{\mathbf{A}})\geq 2\tilde{K}$ [21]. Since we now have a wide matrix $\tilde{\mathbf{A}}$, $\mathrm{krank}\,(\tilde{\mathbf{A}}^*\otimes\tilde{\mathbf{A}})=\ \mathrm{krank}(\tilde{\mathbf{A}})$ [22]. Based on this fact and by exploiting the Vandermonde structure of $\tilde{\mathbf{A}}$, it is clear that the necessary and sufficient condition that needs to be satisfied is given by $N\geq 2\tilde{K}$. For $\mathrm{vec}(\mathbf{R}_{\tilde{s}})$ reconstruction using ℓ_1-norm minimization, the coherence property of $\tilde{\mathbf{A}}^*\otimes\tilde{\mathbf{A}}$ is of particular interest. Given the definition of coherence of $\tilde{\mathbf{A}}$ as $\gamma_{\tilde{\mathbf{A}}}=\max_{i\neq j}|\mathbf{a}(\tilde{\theta}_i)^H\mathbf{a}(\tilde{\theta}_j)|/\|\mathbf{a}(\tilde{\theta}_i)\|\|\mathbf{a}(\tilde{\theta}_j)\|$[23], it is straightforward to show that $\gamma_{\tilde{\mathbf{A}}^*\otimes\tilde{\mathbf{A}}}=\gamma_{\tilde{\mathbf{A}}}$ [22]. As a result, in a noiseless scenario, a loose sufficient condition for a unique reconstruction of $\mathrm{vec}(\mathbf{R}_{\tilde{s}})$ using ℓ_1-norm minimization is given by $\tilde{K}\leq\frac{1}{2}(1+1/\gamma_{\tilde{\mathbf{A}}})$ [23].

4.3. Spatial smoothing and MUSIC

Since we use a ULA of N antennas as our underlying array, it is also possible to apply the spatial smoothing procedure of [2] or [6] to the spatial correlation matrix estimate $\hat{\mathbf{R}}_x$ obtained from (13) or (14). Here, we opt to employ the forward–backward spatial smoothing (FBSS) introduced in [6], which is theoretically able to detect more correlated sources than that can be detected by the forward technique in [2]. Specifically, we divide the underlying ULA into N_s overlapping subarrays, each of which has N_a physical antennas, and compute the $N_a\times N_a$ spatially smoothed correlation matrix $\hat{\bar{\mathbf{R}}}_x$ as

$$[\hat{\bar{\mathbf{R}}}_x]_{i,j}=\frac{1}{N_s}\sum_{i'=0}^{N_s-1}([\hat{\mathbf{R}}_x]_{i+i',j+i'}+[\hat{\mathbf{R}}_x^*]_{N+1-i-i',N+1-j-i'}) \tag{24}$$

where $[\hat{\mathbf{R}}_x]_{i,j}$ represents the element of $\hat{\mathbf{R}}_x$ at the i-th row and the j-th column. We can then apply the MUSIC algorithm of [3] to the resulting $\hat{\bar{\mathbf{R}}}_x$ in order to produce high resolution DOA estimates. It is important to note that a larger N_s implies a smaller N_a and vice versa, and that the maximum number of sources that can be detected by MUSIC after the FBSS preprocessing scheme is given by $\min(2N_s,N_a-1)$ [6]. It is easy to show that for our underlying ULA, the optimal settings for N_s and N_a, which lead to the largest possible number of sources that can be detected, are given by $N_s=\lceil N/3\rceil$ with $N_a=N+1-\lceil N/3\rceil$.

5. Discussion

We first would like to underline some important issues with respect to the LS formulation for DOA estimation discussed in Section 4.1. Recall that in the LS formulation, the limited grid resolution in the angular domain might seriously affect the estimation of the DOA of point sources, especially when it is not located nearby the grid. When this is the case, we might expect MUSIC with spatial smoothing discussed in Section 4.3 to perform better than the LS approach. However, it is important to note that the LS approach also has its own merits. In fact, the gridding performed in the LS method aims at estimating the general angular power spectrum represented by the diagonal of the estimated signal correlation matrix $\mathbf{R}_{\tilde{s}}$, without any sparsity considerations (i.e., by allowing $Q\leq N$). In that sense, our LS approach can actually be interpreted as a conventional periodogram approach used for spectral estimation. Let us for instance consider the case where we have a source that is occupying a whole angular band (e.g., there are no point sources). We then have a conventional spectral estimation problem instead of a line spectrum estimation problem and there is a good chance for the LS approach to outperform MUSIC, which means that the considered LS angular power spectrum reconstruction method is reasonable in some cases. More details can be found in Section 6. Some extensions of MUSIC have been proposed in [24,25] to estimate the DOA of spatially distributed sources but these approaches are not really designed to estimate an arbitrary smooth angular power spectrum.

Both the LS and the sparsity-regularized LS provide information about how the sources are correlated to each other. This information is available in the off-diagonal components of $\mathbf{R}_{\tilde{s}}$ and cannot be produced using the MUSIC approach. With the ability to use LS, sparsity-regularized LS, and MUSIC with spatial smoothing, our dynamic linear array approach has two features that complement each other. The gridding approach assisted with LS is very useful for a smooth angular power spectrum estimation while MUSIC with spatial smoothing is a more appropriate tool for the DOA estimation of point sources. In addition, subject to the sparsity of the angular power spectrum, the sparsity-regularized LS approach is able to produce an estimate of a smooth angular power spectrum as well as accurate DOA estimates for point sources as long as the grid is sufficiently fine.

The fact that $\mathrm{diag}(\hat{\mathbf{R}}_{\tilde{s}})$ provides the estimate of the received power at the investigated angles $\{\tilde{\theta}_q\}_{q=1}^{Q}$ can also be used as a motivation to add a positivity constraint on $\mathrm{diag}(\mathbf{R}_{\tilde{s}})$ in the ordinary LS problem discussed in Section 4.1. This leads to the following constrained LS problem:

$$\hat{\mathbf{R}}_{\tilde{s}}=\arg\min_{\mathbf{R}_{\tilde{s}}}\|\mathrm{vec}(\mathbf{R}_x)-(\tilde{\mathbf{A}}^*\otimes\tilde{\mathbf{A}})\mathrm{vec}(\mathbf{R}_{\tilde{s}})\|_2^2\quad\text{s.t. }\mathrm{diag}(\mathbf{R}_{\tilde{s}})\geq\mathbf{0}_Q \tag{25}$$

with $\mathbf{0}_n$ denoting an $n\times 1$ vector containing only zeros. Furthermore, if a higher computational complexity is acceptable, we can even apply a p.s.d. constraint on $\mathbf{R}_{\tilde{s}}$, which means that the constrained LS problem in (25) now becomes

$$\hat{\mathbf{R}}_{\tilde{s}}=\arg\min_{\mathbf{R}_{\tilde{s}}}\|\mathrm{vec}(\mathbf{R}_x)-(\tilde{\mathbf{A}}^*\otimes\tilde{\mathbf{A}})\mathrm{vec}(\mathbf{R}_{\tilde{s}})\|_2^2\quad\text{s.t. }\mathbf{R}_{\tilde{s}}\succcurlyeq\mathbf{0}_{Q\times Q}. \tag{26}$$

Similarly, we can also add a positivity or p.s.d. constraint on $\mathrm{diag}(\mathbf{R}_{\tilde{s}})$ in (23) for the sparsity-regularized LS approach discussed in Section 4.2.

Another interesting observation is that the LS and sparsity-regularized LS approaches can also be adapted to their one-step counterparts. Instead of first solving (11) to reconstruct $\mathbf{R}_x$ from $\mathbf{r}_y$ and then (20) to reconstruct $\mathbf{R}_{\tilde{s}}$ from $\mathbf{R}_x$, it is actually possible to reconstruct $\mathbf{R}_{\tilde{s}}$ directly

from $\mathbf{r}_y$ in (11). This is performed by combining (11) and (20) and solving the resulting problem using a single LS or sparsity-regularized LS operation. More specifically, we can write

$$\mathbf{r}_y = \mathbf{\Psi}(\tilde{\mathbf{A}}^* \otimes \tilde{\mathbf{A}})\mathrm{vec}(\mathbf{R}_{\tilde{s}}) + \sigma_n^2 \mathbf{\Psi}\mathrm{vec}(\mathbf{I}_N) = \mathbf{G}\mathrm{vec}(\mathbf{R}_{\tilde{s}}) + \sigma_n^2 \mathbf{\Psi}\mathrm{vec}(\mathbf{I}_N) \tag{27}$$

where the $M^2L \times Q^2$ matrix $\mathbf{G}$ is given by

$$\mathbf{G} = [((\mathbf{C}_0\tilde{\mathbf{A}})^* \otimes (\mathbf{C}_0\tilde{\mathbf{A}}))^T, ((\mathbf{C}_1\tilde{\mathbf{A}})^* \otimes (\mathbf{C}_1\tilde{\mathbf{A}}))^T, \ldots, ((\mathbf{C}_{L-1}\tilde{\mathbf{A}})^* \otimes (\mathbf{C}_{L-1}\tilde{\mathbf{A}}))^T]^T. \tag{28}$$

From this equation, we can directly adopt a one-step LS or sparsity-regularized LS to reconstruct $\mathrm{vec}(\mathbf{R}_{\tilde{s}})$ from $\mathbf{r}_y$. We expect that the corresponding reconstruction conditions, i.e., full column rank condition on $\mathbf{G}$ for LS and $\mathrm{krank}(\mathbf{G}) \geq 2\tilde{K}$ or $\tilde{K} \leq \frac{1}{2}(1 + 1/\gamma_{\mathbf{G}})$ conditions for sparsity-regularized LS, will be less strict than in the two-step approaches. However, since it is not directly clear what properties are required to obtain these conditions for the one-step approaches, we generally advocate to first solve (11) and then reconstruct $\mathbf{R}_{\tilde{s}}$ from (20) using LS or sparsity-regularized LS.

6. Numerical study

In this section, we evaluate the proposed approaches using numerical experiments. In general, we run the proposed dynamic array through periodic scanning discussed in Section 2 and then reconstruct the spatial correlation matrix $\mathbf{R}_x$ from $\mathbf{r}_y$ in (11) using ordinary LS except for the last experiment where we use (14) to reconstruct $\mathbf{R}_x$. Next, given the estimate of $\mathbf{R}_x$, we evaluate the main source correlation matrix reconstruction and DOA estimation approaches elaborated in Section 4. For all experiments, we also apply the positivity constraint on the diagonal elements of $\mathbf{R}_{\tilde{s}}$ when we adopt the sparsity-regularized LS since adding this convex constraint does not incur a large computational cost. In general, we consider correlated sources as well as a spatially and temporally white noise, and we assume that the signals coming from different sources have equal power with the signal to noise ratio (SNR) defined with respect to the power of each signal at each antenna.

Under an SNR of 0 dB, we first conduct three experiments and examine the resulting LS, sparsity-regularized LS, and MUSIC angular power spectrum plots. In the first experiment, we consider a ULA of $N=40$ antennas with half wavelength spacing as our underlying array and set the number of time slots per scanning period to $L=28$. We intend to select the activated antennas in each time slot such that the number of active antennas per time slot M is minimal. Observe that, according to (19), the lower bound for M in this setting is given by $M \geq 8$. In this simulation study however, we run Algorithm 2 given in Table 2 for $N=40$ and $L=28$ in order to obtain a sub-optimal solution for M and the indices of the antennas that are activated in each time slot, which is given by $\{\Gamma_l\}_{l=0}^{27}$. This results in $M=10$ (which is larger than the lower bound) and produces the indices of the corresponding 10 active antennas in each of the 28 time slots. Note that the antenna array setup suggested by $\{\Gamma_l\}_{l=0}^{27}$ produced by Algorithm 2 leads to a full column rank 2800×1600 matrix $\mathbf{\Psi}$ in (12). The total number of time samples per time slot is $S=1$ and the total number of scanning periods is $P=57$ leading to a total number of time samples of $PSL=1596$. For the LS approach, we set the number of grid points to $Q=N=40$ and the investigated angles $\{\tilde{\theta}_q\}_{q=1}^{40}$ according to (22) in order to produce a well-conditioned matrix $\tilde{\mathbf{A}}^* \otimes \tilde{\mathbf{A}}$ in (20). The number of grid points for the sparsity-regularized LS approach is equal to $Q=70$ and they are also set according to (22). For the sparsity-regularized LS, the weight λ in (23) is set to $\lambda = 2.88$. For the MUSIC approach, the FBSS preprocessing scheme is conducted by setting the number of subarrays to $N_s=14$ and the number of antennas per subarray to $N_a=27$. We generate $K=12$ sources with 9 degrees of separation, that is $\{\theta_k\}_{k=1}^{12} = \{-54^\circ, -45^\circ, \ldots, 45^\circ\}$. Note that the number of sources is more than the number of active antennas per time slot M. In order to investigate the performance of the proposed approach for the case when there is some correlation between the sources, the signal that arrives at angle θ_k is set to be exactly the same as the one arriving at direction θ_{k+6} leading to six pairs of fully correlated sources. The diagonal of $\hat{\mathbf{R}}_{\tilde{s}}$ recovered using ordinary LS and sparsity-regularized LS gives the angular power spectrum estimates at the investigated angles $\tilde{\theta}_q$ and is illustrated in Fig. 3. In this figure, the locations of the actual DOAs are indicated by vertical lines for simplicity. We then use the 12 highest peaks in the resulting angular power spectrum estimate to indicate the DOA estimates. We can see how the 12 correlated sources can generally be detected using ordinary LS since they are located nearby the LS grid points. Meanwhile, the sparsity-regularized LS produces a minor grid mismatch effect but has less power in the unoccupied angular band. The resulting MUSIC estimate is also illustrated in Fig. 3 and it generally outperforms both the LS estimate and sparsity-regularized LS estimate. It should be noted, however, that both the LS and the sparsity-regularized LS also provide information about the magnitude of the correlation

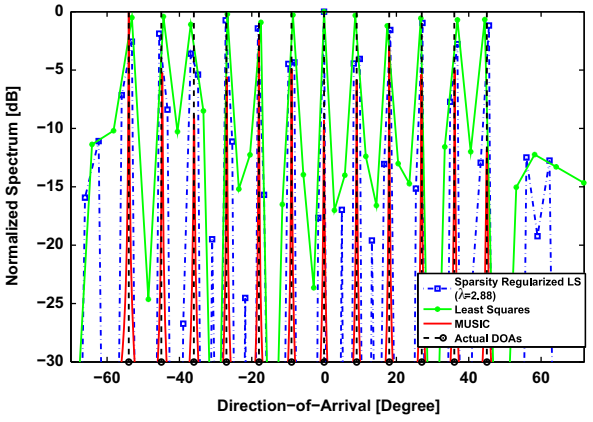

Fig. 3. Normalized spectrum (dB) of the MUSIC, LS, and sparsity-regularized LS approaches versus DOA (degree) for the first experiment. We have $K=12$ sources, $N=40$, $L=28$, $M=10$, $P=57$ and SNR=0 dB. For the LS and sparsity-regularized LS approaches, we have $Q=40$ and $Q=70$, respectively.

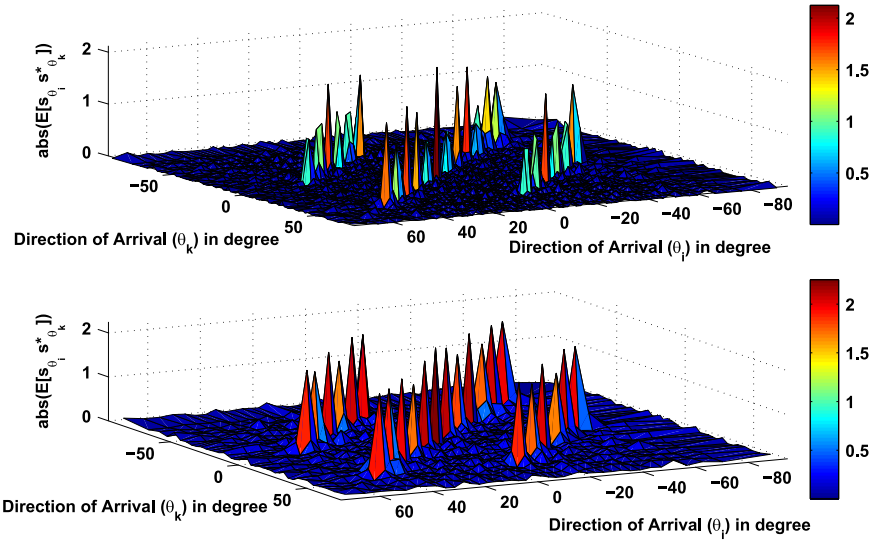

Fig. 4. The magnitude of the elements of the estimated correlation matrix $\hat{\mathbf{R}}_{\tilde{s}}$ computed using the sparsity-regularized LS (top) and the LS (bottom) approaches for the first experiment. Here $K=12$, SNR$=0$ dB, $N=40$, $M=10$, $P=57$, and $L=28$. For the LS and sparsity-regularized LS approaches, we have $Q=40$ and $Q=70$, respectively.

between the signals at the different investigated angles $\tilde{\theta}_q$, which is provided in Fig. 4. As it is clear from the figure, both the power of the 12 sources and the magnitude of the cross-correlation between the sources are clearly identified by both the LS and the sparsity-regularized LS approaches.

In the second experiment, we consider a ULA of $N=25$ antennas with half wavelength spacing as our underlying array. We activate $M=5$ active antennas in each time slot and run Algorithm 1 given in Table 1, which produces $L=36$ and the indices of the corresponding 5 active antennas in each of the 36 time slots. The grid points setting for the sparsity-regularized LS is the same as in the first experiment while for the LS approach, we have $Q=N=25$ where $\{\tilde{\theta}_q\}_{q=1}^{25}$ is set based on (22). Here, the weight λ in (23) for the sparsity-regularized LS is set to $\lambda=3.88$. For the MUSIC approach, the FBSS preprocessing scheme is conducted by setting the number of subarrays to $N_s=9$ and the number of antennas per subarray to $N_a=17$. We maintain $S=1$ but have $P=44$, which leads to a total number of time samples of $PSL=1584$. We now generate three pairs of fully correlated sources leading to $K=6$ sources having DOAs with 10 degrees of separation, that is $\{\theta_k\}_{k=1}^{6}=\{-2.97^\circ, 7.03^\circ, \ldots, 47.03^\circ\}$. Note that we again have more sources than active antennas per time slot M. Fig. 5 illustrates the angular power spectrum estimates. Again, the location of the actual DOAs is indicated by vertical lines. Observe that for this realization, the accuracy of the DOA estimates produced by the sparsity-regularized LS is quite comparable to that of the MUSIC estimates though the sparsity-regularized LS approach introduces a significant amount of power in the unoccupied angular band. The ordinary LS DOA estimates, on the other hand, introduce a significant amount of grid mismatch due to a coarse grid of investigated angles. Fig. 6 describes the magnitude of the correlation between the signals at the different investigated angles $\tilde{\theta}_q$ estimated

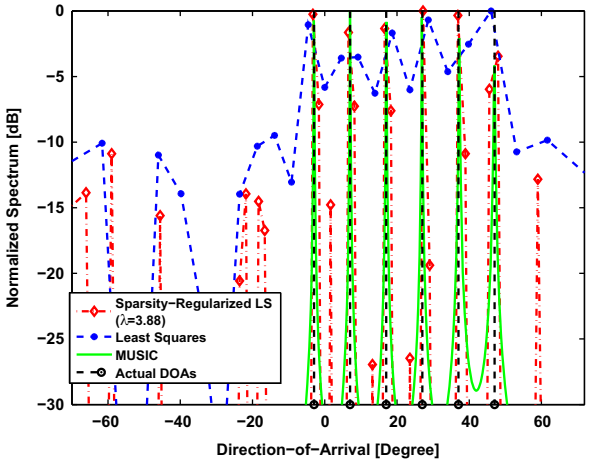

Fig. 5. Normalized spectrum (dB) of the MUSIC, LS, and sparsity-regularized LS approaches versus DOA (degree) for the second experiment. We have $K=6$ sources, $N=25$, $L=36$, $M=5$, $P=44$, and SNR$=0$ dB. For the LS and sparsity-regularized LS approaches, we have $Q=25$ and $Q=70$, respectively.

using the ordinary LS (bottom part) and the sparsity-regularized LS (top part) approaches. As it is clear from the figure, both the power of the six sources and the magnitude of the cross-correlation between the sources are better identified by the sparsity-regularized LS than by the ordinary LS approach.

All simulation settings for the third experiment are similar to those for the first experiment, but we now consider a continuous source from 30° to 40°, which is simulated by generating 250 pairs of fully correlated sources with 0.02° of separation. The parameter λ for the sparsity-regularized LS is set to $\lambda=0.012$. The result is illustrated in Fig. 7. The MUSIC algorithm clearly fails for this continuous source scenario while the sparsity-regularized

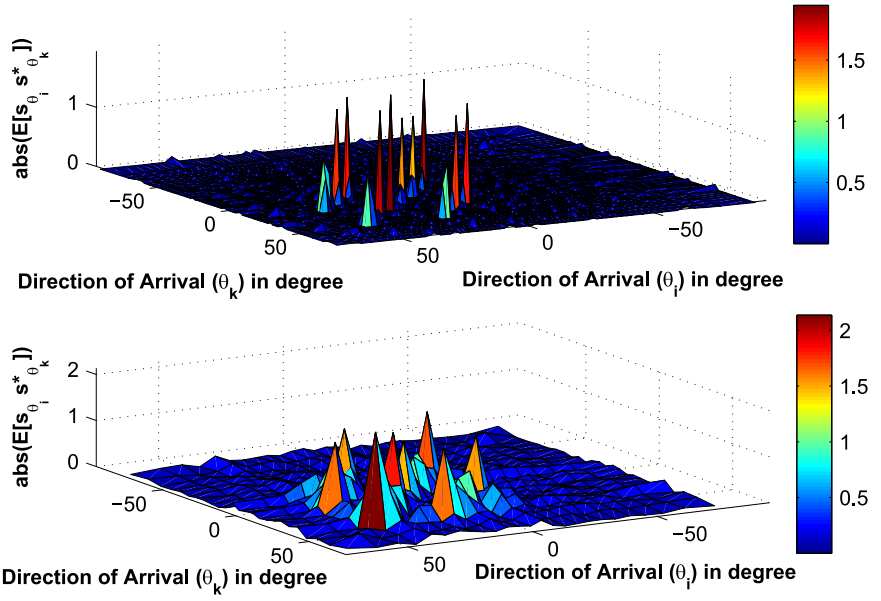

Fig. 6. The magnitude of the elements of the estimated correlation matrix $\hat{\mathbf{R}}_{\tilde{s}}$ computed using the sparsity-regularized LS (top) and LS (bottom) approaches for the second experiment. Here $K=6$, SNR$=0$ dB, $N=25$, $M=5$, $P=44$, and $L=36$. For the LS and sparsity-regularized LS approaches, we have $Q=25$ and $Q=70$, respectively.

LS and LS approaches better reconstruct the continuous angular range where lower sidelobes and a better resolution are found for the sparsity-regularized LS.

The dynamic array, the FBSS, and the angular grid setting of the second experiment is now used in the fourth experiment to compute the root mean square error (RMSE) between the actual DOAs and the DOA estimates. The DOAs of three pairs of fully coherent sources are randomly generated between -60° and 60° but with a fixed 10° of separation. With $S=1$ and SNR $=0$ dB, we first vary P from $P=4$ to $P=100$. Based on the resulting spectrum, we locate the six highest peaks. For every source, we compute the RMSE between the true DOA and the peak that is closest to this DOA, selected from the earlier determined six highest peaks. Fig. 8 illustrates the computed RMSE for the three approaches for a varying P. Observe how the performance of the ordinary LS approach is quite poor due to its limited grid resolution. The performance of the sparsity-regularized LS approach is much better than the ordinary LS approach but it tends to flatten at a particular level which is determined by the resolution of the 70 grid points used by this approach. Meanwhile, the MUSIC approach performs better than the two aforementioned approaches and its RMSE continues to decrease as P increases. A similar situation is also found in Fig. 9, where we fix the total number of scanning periods to $P=7$ and vary the SNR. In this scenario, however, the performance of the sparsity-regularized LS has not yet hit the saturation point defined by the resolution of its 70 grid points. In fact, its RMSE continues to decrease as the SNR varies from -10 dB to 0 dB.

A much better performance in terms of RMSE for LS is found when we increase N and Q to $N=Q=40$ as shown in Fig. 10. In this fifth experiment, we only focus on the LS and MUSIC approaches. Here, we have $M=7$ and run Algorithm 1 to produce $L=48$. We vary P from $P=1$ to $P=40$ and the SNR

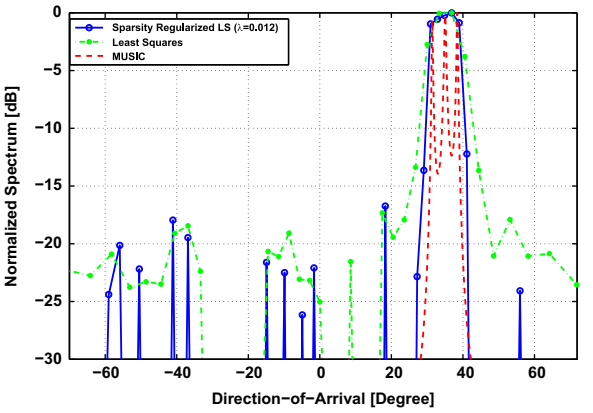

Fig. 7. Normalized spectrum (dB) of the MUSIC, LS, and sparsity-regularized LS approaches versus DOA (degree) for the third experiment. Here we have $K=500$ sources with DOAs between 30° and 40°, SNR$=0$ dB, $N=40$, $M=10$, and $L=28$. For the LS and sparsity-regularized LS approaches, we have $Q=40$ and $Q=70$, respectively.

from -10 dB to 0 dB. The FBSS setting for MUSIC is the same as in the first experiment and there are four pairs of fully correlated sources (which again implies $K>M$) whose DOAs are generated in the same way as in the fourth experiment. Note how the performance of the ordinary LS approach is mainly dictated by the grid resolution.

In the last experiment, we investigate the impact of applying the p.s.d. constraint on the reconstructed $\mathbf{R}_x$ (see (14)) and focus on the performance of the MUSIC approach by considering different settings of the dynamic array. In general, we set the number of active antennas per time slot to $M=3$ and examine three different dynamic array settings, i.e., $N=17$, $N=14$, and $N=11$. Given $M=3$, we execute Algorithm 1 in Table 1 for $N=17$, $N=14$, and $N=11$, leading to $L=47$, $L=33$,

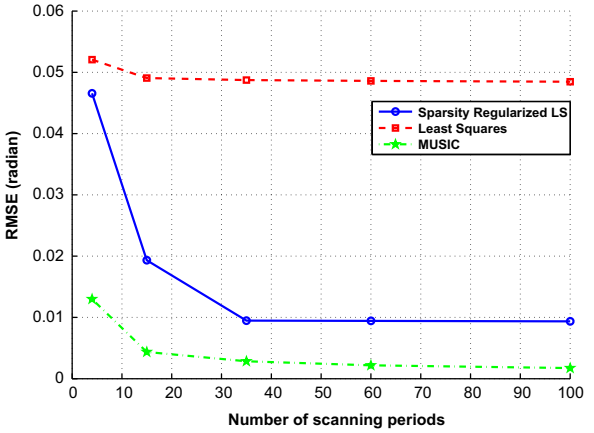

Fig. 8. The performance of LS, sparsity-regularized LS and MUSIC DOA estimates for different scanning periods P. Here we have SNR $=0$ dB, $N=25$, $M=5$, $L=36$, and $K=6$ correlated sources whose DOAs are randomly generated with 10° of separation. For the LS and sparsity-regularized LS approaches, we have $Q=25$ and $Q=70$, respectively.

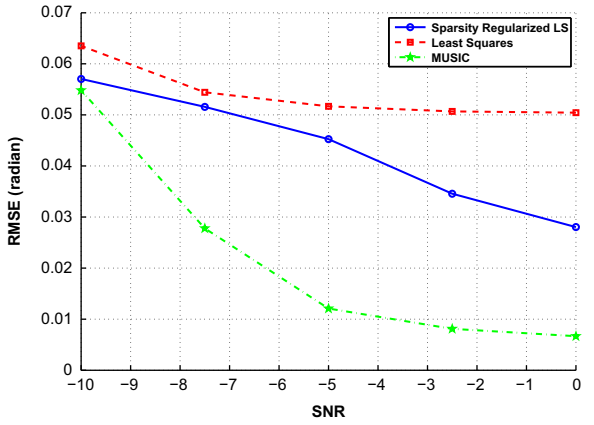

Fig. 9. The performance of the LS, sparsity-regularized LS and MUSIC DOA estimates for different SNRs. Here we have $P=7$, $N=25$, $M=5$, $L=36$, and $K=6$ correlated sources whose DOAs are randomly generated with 10° of separation. For the LS and sparsity-regularized LS approaches, we have $Q=25$ and $Q=70$, respectively.

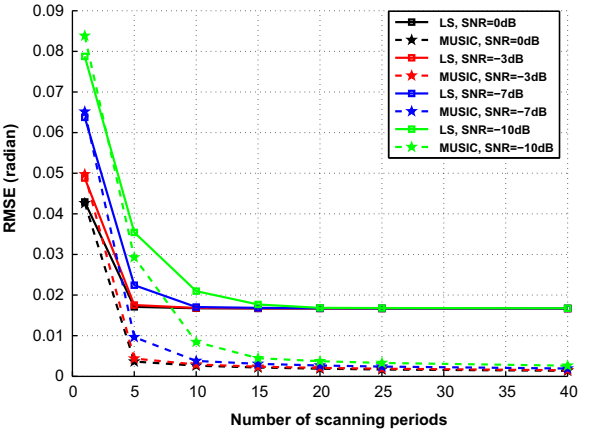

Fig. 10. The performance of the LS and MUSIC DOA estimates for different SNRs and scanning periods P. Here we have $N=Q=40$, $M=7$, $L=48$, and $K=8$ correlated sources whose DOAs are randomly generated with 10° of separation.

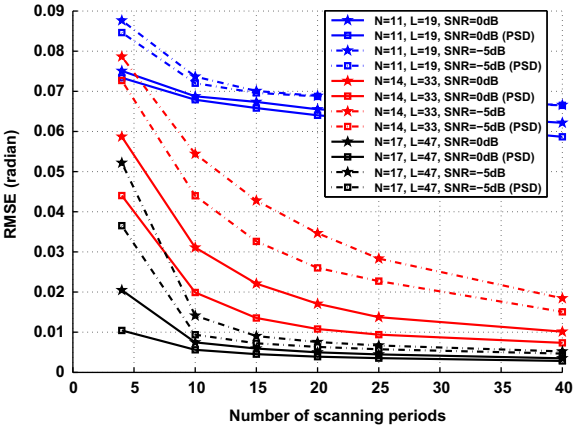

Fig. 11. The impact of the p.s.d. constraint on the reconstructed $\mathbf{R}_x$. Here, we focus on the MUSIC DOA estimates for different settings of the dynamic array (different N and L) as well as different SNRs and scanning periods P using $M=3$ active antennas. Here we have $K=4$ correlated sources whose DOAs are randomly generated with 10° of separation.

and $L=19$, respectively. For the FBSS process, it is important to note that for different values of N, we also have different optimal values of N_s and N_a. Here, we compute N_s and N_a as $N_s=\lceil N/3\rceil$ and $N_a=N+1-\lceil N/3\rceil$, respectively (as suggested in Section 4.3). With $S=1$, we vary P between $P=4$ and $P=40$. On top of that, we also evaluate two different SNR values, i.e., SNR $=0$ dB and SNR $=-5$ dB. We generate two pairs of fully correlated sources ($K=4$) and compute the RMSE between the actual and the estimated DOAs by following the same procedure introduced in the fourth experiment. Fig. 11 illustrates the computed RMSE for this experiment. As expected, the performance of the MUSIC approach for all dynamic array settings gets worse for lower SNR. We can see that applying the p.s.d. constraint on the reconstructed $\mathbf{R}_x$ indeed improves the performance, especially for $N=14$. It is interesting to observe that, for a given SNR, a larger performance degradation is experienced when we reduce $N=14$ and $L=33$ to $N=11$ and $L=19$, respectively, than when we reduce it from $N=17$ and $L=47$ to $N=14$ and $L=33$, respectively. In fact, when $N=11$, we only have $N_s=4$ subarrays of $N_a=8$ antennas. According to the theoretical analysis in [6], this setting should still be able to estimate $\min(2N_s, N_a-1)=7$ correlated sources. However, in practice, we observe that there are a few occasions where there is only a small difference between the value of the fourth largest eigenvalue and that of the noise eigenvalues of the resulting spatially smoothed matrix $\bar{\mathbf{R}}_x$ in (24). As a result, the MUSIC approach might not be able to separate the fourth signal eigenvector from the noise subspace. Observe that, for $N=11$, applying the p.s.d. constraint on the reconstructed $\mathbf{R}_x$ only offers a small improvement.

7. Conclusions

In this paper, we have developed a new method to estimate the DOA of possibly fully correlated sources based on second-order statistics by adopting a so-called dynamic array, which is formed by performing a periodic scanning

of an underlying ULA having N available antennas. Here, different sets of M antennas are activated in different time slots. We first collect the spatial correlation matrices of the output of the antenna arrays for all time slots and present them as a linear function of the spatial correlation matrix $\mathbf{R}_x$. We then present the theoretical condition that needs to be satisfied to ensure the full column rank condition of the system matrix, which later allows us to reconstruct $\mathbf{R}_x$ using LS. Note that, apart from our dynamic array approach which allows for $\mathbf{R}_x$ reconstruction using LS, it is also possible to use low-rank matrix completion to reconstruct $\mathbf{R}_x$ under a finite number of measurements. This, for instance, is discussed in [26]. However, this topic is beyond the scope of our paper and we consider this as a possible topic for future research. Based on the estimated $\mathbf{R}_x$, we propose three different options. The first option is to define an angular grid of investigated angles where the number of grid points Q is less than or equal to the number of physical antennas N in the underlying array. This allows us to reconstruct the correlation matrix of the incident signals at the investigated angles using LS subject to the full column rank condition of the system matrix. Since the LS signal correlation matrix reconstruction is vulnerable to a grid mismatch effect due to the limited grid resolution, we propose a sparsity-regularized LS approach as the second option and increase the grid resolution by allowing $Q \gg N$. However, this option theoretically works well only when the actual angular power spectrum is sparse. The last option is to apply FBSS on the reconstructed $\mathbf{R}_x$ and use the MUSIC algorithm based on the spatially smoothed correlation matrix. This option might produce high resolution DOA estimates but does not provide information about how the sources are correlated to each other. In general, our dynamic array approach can estimate the DOAs of the impinging signals even when the number of correlated sources is larger than the number of active antennas per time slot. The simulation study has indicated that our method performs satisfactory even when some sources are fully coherent.

Appendix A. Proof of Lemma 1

Let us assume that $\mathbf{e}_i^T$ and $\mathbf{e}_j^T$ are the i-th and the j-th rows of $\mathbf{I}_N$, respectively. It is easy to check that for any $i,j \in \{1,2,\ldots,N\}$, the Kronecker product $\mathbf{e}_i^T \otimes \mathbf{e}_j^T$ results in a $1 \times N^2$ vector having a single one at the $[(i-1)N+j]$−th position. Correspondingly, $\mathbf{e}_j^T \otimes \mathbf{e}_i^T$ produces a $1 \times N^2$ vector having a single one at the $[(j-1)N+i]$−th position. As a result, if $\mathbf{C}_l$ has $\mathbf{e}_i^T$ and $\mathbf{e}_j^T$ as two of its rows, $\mathbf{C}_l \otimes \mathbf{C}_l$ will definitely have a one in the $[(i-1)N+j]$−th and $[(j-1)N+i]$−th columns. This proves the sufficiency part of the lemma. In order to prove the necessity part, let us assume that $\mathbf{C}_l \otimes \mathbf{C}_l$ has a one in the $[(i-1)N+j]$−th column but either the i-th row of $\mathbf{I}_N$, the j-th row of $\mathbf{I}_N$, or both of them are missing from $\mathbf{C}_l$. Further assume that the row of $\mathbf{C}_l \otimes \mathbf{C}_l$ having a one in the $[(i-1)N+j]$−th column is produced by the Kronecker product operation between two rows of $\mathbf{C}_l$ taken from the a-th and the b-th rows of $\mathbf{I}_N$, i.e., $\mathbf{e}_a^T \otimes \mathbf{e}_b^T$. Now, $\mathbf{e}_a^T \otimes \mathbf{e}_b^T$ results in a $1 \times N^2$ vector having a single one at the $[(a-1)N+b]$−th position. Therefore, it is obvious that $a=i$ and $b=j$. In other words, the i-th and the j-th rows of $\mathbf{I}_N$ are not missing from $\mathbf{C}_l$, which is a contradiction. A similar proof applies for the row of $\mathbf{C}_l \otimes \mathbf{C}_l$ that has a single one in the $[(j-1)N+i]$−th column. This concludes the proof of this lemma.

Appendix B. Explanation for Algorithm 1 (see Table 1)

We use the indicator matrix $\mathbf{Z}^{(f)}$ in Table 1 to indicate whether a certain combination of two antennas has been activated in at least one of the first f time slots. Specifically, $[\mathbf{Z}^{(f)}]_{i,j}=0$ implies that a combination of the i-th and the j-th antennas has never been simultaneously activated in the first f time slots whereas $[\mathbf{Z}^{(f)}]_{i,j}=1$ indicates that the combination of the i-th and the j-th antennas has been simultaneously activated at least once in the first f time slots. Consequently, it is also obvious that $\mathbf{Z}^{(f)}$ is a symmetric matrix. Based on Theorem 1, our objective is to guarantee that every possible combination of two antennas in the underlying ULA is active in at least one of the L possible time slots within a scanning period. In other words, we are only interested in the off-diagonal components of $\mathbf{Z}^{(f)}$ and thus, we initialize $\mathbf{Z}^{(f)}$ with $\mathbf{Z}^{(0)}=\mathbf{I}_N$.

In general, Algorithm 1 consists of L main iterations indicated by a while loop in Table 1. The reason to use a while loop to implement the main iterations is due to the fact that L is unknown. The objective of the while loop is to choose M antennas for each time slot. One main iteration corresponds to the selection of M antennas for one time slot. The first task in the main iteration (see step 5 in Table 1) is to randomly select a combination of two antennas that has not been used in the previous time slot.

The task of the inner for loop in Table 1, which consists of $M-2$ iterations, is to choose the remaining $M-2$ antennas for the considered time slot. For each antenna selection, our aim is to maximize the number of conversion of zeros in $\mathbf{Z}^{(f)}$ to ones. This is done because we want to ensure that each antenna selection results in a maximum number of new combinations of two active antennas that have not been simultaneously used in the previous time slots.

Note that the main iterations will stop once every possible pair of two antennas has been selected for at least one time slot.

Appendix C. Explanation for Algorithm 2 (see Table 2)

For Algorithm 2 in Table 2, we use a similar notation to the one used for Algorithm 1. However, in this algorithm, all time slots are considered simultaneously and thus we now use $\mathbf{Z}^{(f)}$ to indicate whether a certain combination of two antennas has been used as two of the first $f+1$ active antennas in any time slot. The task of the first for loop in Algorithm 2 is to select the first two antennas for each time slot. One iteration corresponds to the selection of the first two antennas for one time slot. Once we have selected the first two active antennas for each time slot, we proceed to the while loop indicated by steps 8–16 in Table 2. Here, one iteration of the while loop corresponds to the selection of one additional antennas for all time slots. The reason to use while loop here is due to the fact that M is not known. The inner for loop inside the while loop

performs the selection of one additional antenna for one time slot in each iteration. As in Algorithm 1, each antenna selection aims to maximize the number of conversion of zeros in $\mathbf{Z}^{(f)}$ to ones.

References

[1] P.P. Vaidyanathan, P. Pal, Direct-MUSIC on sparse arrays, in: Proceedings of International Conference on Signal Processing and Communications (SPCOM), Bangalore, India, July 2012.

[2] T.J. Shan, M. Wax, T. Kailath, On spatial smoothing for direction-of-arrival estimation of coherent signals, IEEE Transactions on Acoustics, Speech, and Signal Processing 33 (August (4)) (1985) 806–811.

[3] R.O. Schmidt, Multiple emitter location and signal parameter estimation, IEEE Transactions on Antennas and Propagation 34 (March (3)) (1986) 276–280.

[4] A.J. Barabell, Improving the resolution performance of eigenstructure-based direction-finding algorithm, in: Proceedings of IEEE International Conference on Acoustics, Speech, and Signal Processing, Boston, Massachusetts, April 1983, pp. 336–339.

[5] J.A. Cadzow, A high resolution direction-of-arrival algorithm for narrow-band coherent and incoherent sources, IEEE Transactions on Acoustics, Speech, and Signal Processing 36 (July (7)) (1988) 965–979.

[6] S.U. Pillai, B.H. Kwon, Forward/backward spatial smoothing techniques for coherent signal identification, IEEE Transactions on Acoustics, Speech, and Signal Processing 37 (January (1)) (1989) 8–15.

[7] D. Malioutov, M. Cetin, A.S. Willsky, A sparse signal reconstruction perspective for source localization with sensor arrays, IEEE Transactions on Signal Processing 53 (August (8)) (2005) 3010–3022.

[8] M.M. Hayder, K. Mahata, Direction-of-arrival estimation using a mixed $\ell_{2,0}$ norm approximation, IEEE Transactions on Signal Processing 58 (September (9)) (2010) 4646–4655.

[9] J. Yin, T. Chen, Direction-of-arrival estimation using a sparse representation of array covariance vectors, IEEE Transactions on Signal Processing 59 (September (9)) (2011) 4489–4493.

[10] P. Stoica, P. Babu, J. Li, New method of sparse parameter estimation in separable models and its use for spectral analysis of irregularly sampled data, IEEE Transactions on Signal Processing 59 (January (1)) (2011) 35–47.

[11] P. Stoica, P. Babu, J. Li, SPICE: a sparse covariance-based estimation method for array processing, IEEE Transactions on Signal Processing 59 (February (2)) (2011) 629–638.

[12] S.U. Pillai, Y. Bar-Ness, F. Haber, A new approach to array geometry for improved spatial spectrum estimation, Proceeding of the IEEE 73 (October (10)) (1985) 1522–1524.

[13] S.U. Pillai, F. Haber, Statistical analysis of a high resolution spatial spectrum estimator utilizing an augmented covariance matrix, IEEE Transactions on Acoustics, Speech, and Signal Processing 35 (November (11)) (1987) 1517–1523.

[14] Y.I. Abramovich, D.A. Gray, A.Y. Gorokhov, N.K. Spencer, Positive-definite Toeplitz completion in DOA estimation for nonuniform linear antenna arrays—part I: fully augmentable arrays, IEEE Transactions on Signal Processing 46 (September (9)) (1998) 2458–2471.

[15] W. Ma, T. Hsieh, C. Chi, DOA estimation of quasi-stationary signals via Khatri-Rao subspace, in: Proceedings of IEEE International Conference on Acoustics, Speech, and Signal Processing, Taipei, Taiwan, April 2009, pp. 2165–2168.

[16] S. Shakeri, D.D. Arianandа, G. Leus, Direction of arrival estimation using sparse ruler array design, in: Proceedings of the 13th IEEE International Workshop on Signal Processing Advances in Wireless Communications, Cesme, Turkey, June 2012.

[17] P. Pal, P.P. Vaidyanathan, Correlation-aware techniques for sparse support recovery, in: Proceedings of IEEE Statistical Signal Processing (SSP) Workshop, Ann Arbor, Michigan, August 2012, pp. 53–56.

[18] P. Pal, P.P. Vaidyanathan, Nested arrays: a novel approach to array processing with enhanced degrees of freedom, IEEE Transactions on Signal Processing 58 (August (8)) (2010) 4167–4181.

[19] P. Pal, P.P. Vaidyanathan, Coprime sampling and the MUSIC algorithm, in: Proceedings of IEEE Digital Signal Processing and Signal Processing Education Workshop, Sedona, Arizona, January 2011, pp. 289–294.

[20] E. Gonen, M.C. Dogan, J.M. Mendel, Applications of cumulants to array processing: direction-finding in coherent signal environment, in: Proceedings of the 28-th Asilomar Conference on Signal, Systems and Computers, Pacific Grove, California, November 1994, pp. 633–637.

[21] D.L. Donoho, M. Elad, Optimally sparse representation in general nonorthogonal dictionaries via ℓ_1 minimization, Proceedings of National Academy of Sciences of the United States of America 100 (March (5)) (2003) 2197–2202.

[22] S. Jokar, V. Mehrmann, Sparse solutions to underdetermined Kronecker product systems, Elsevier Linear Algebra and its Applications 431 (December (12)) (2009) 2437–2447.

[23] D.L. Donoho, M. Elad, V.N. Temlyakov, Stable recovery of sparse overcomplete representation in the presence of noise, IEEE Transactions on Information Theory 52 (January (1)) (2006) 6–18.

[24] M. Bengtsson, B. Ottersten, Low-complexity estimators for distributed sources, IEEE Transactions on Signal Processing 48 (August (8)) (2000) 2185–2194.

[25] Q. Wu, K. Wong, Y. Meng, W. Read, DOA estimation of point and scattered sources—vec-MUSIC, in: Proceedings of the IEEE 7th SP Workshop on Statistical Signal and Array Processing, Quebec City, Canada, June 1994, pp. 365–368.

[26] A. Waters, V. Cevher, Distributed bearing estimation via matrix completion, in: Proceedings of 2010 IEEE International Conference on Acoustics, Speech, and Signal Processing (ICASSP), Dallas, Texas, March 2010, pp. 2590–2593.